Inorganic Chemistry

Article

pubs.acs.org/IC

Mixed-Lanthanoid Metal–Organic Framework for Ratiometric Cryogenic Temperature Sensing

Xue Liu,[†] Sebastiaan Akerboom,[†] Mathijs de Jong,[‡] Ilpo Mutikainen,[§] Stefania Tanase,[∥] Andries Meijerink,[‡] and Elisabeth Bouwman*[,†]

[†]Leiden Institute of Chemistry, Leiden University, P.O. Box 9502, 2300 RA Leiden, The Netherlands

[‡]Debye Institute for Nanomaterials Science, Utrecht University, Princetonplein 5, 3584 CC Utrecht, The Netherlands

[§]Department of Chemistry, University of Helsinki, P.O. Box 55, A.I. Virtasenaukio 1, FI-00014 Helsinki, Finland

[∥]Van't Hoff Institute for Molecular Sciences, University of Amsterdam, Science Park 904, 1098 XH Amsterdam, The Netherlands

Supporting Information

ABSTRACT: A ratiometric thermometer based on a mixed-metal Ln^{III} metal–organic framework is reported that has good sensitivity in a wide temperature range from 4 to 290 K and a quantum yield of 22% at room temperature. The sensing mechanism in the europium-doped compound $Tb_{0.95}Eu_{0.05}HL$ (H_4L = 5-hydroxy-1,2,4-benzenetricarboxylic acid) is based not only on phonon-assisted energy transfer from Tb^{III} to Eu^{III} centers, but also on phonon-assisted energy migration between neighboring Tb^{III} ions. It shows good performance in a wide temperature range, especially in the range 4–50 K, reaching a sensitivity up to 31% K^{-1} at 4 K.

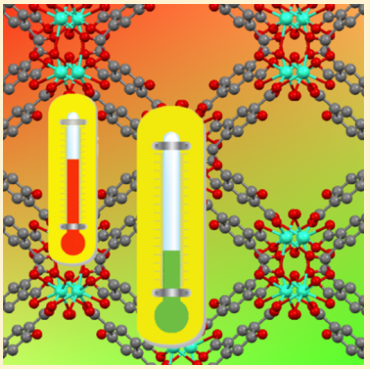

INTRODUCTION

In recent years, lanthanoid metal–organic frameworks (Ln-MOFs) have emerged as very promising multifunctional materials because of the attractive topology structures and their unique luminescence properties, such as the well-defined line emissions, high quantum yields, and long emission lifetimes.[1] A variety of Ln-MOFs has been studied for, e.g., sensing of small organic molecules, temperature sensing, gas storage and separation, proton conduction, and heterogeneous catalysis.[2−5]

Temperature is the most important physical property in both science and industry.[6] Temperature-dependent emission of lanthanoid ions is a key feature for developing new temperature sensors, as changes in temperature can be reflected by the changes of luminescence intensity and lifetime.[2] The luminescent lanthanoid thermometer shows the advantages of fast response, high sensitivity, noninvasive operation, and inertness to strong electric or magnetic fields.[7−9] Compared to lifetime measurements, emission intensity measurements are more straightforward and readily carried out. Most of the emissive temperature sensors are based on only one type of lanthanoid ion. However, their accuracy is easily influenced by the light source intensity, excitation power, and the drifts of the optoelectronic system.[9] It is possible to avoid these drawbacks by referring the temperature to the intensity ratios of selected emission peaks rather than to individual peaks.[2] Two methods have been reported on the basis of luminescence transitions of Eu^{III} and Tb^{III} coordination compounds, or Er^{III}/Yb^{III} nanoparticles.[10] The main advantage is that a single emission spectrum contains all the information needed to compute the absolute temperature.[5]

With the development of aerospace, superconducting magnets, and nuclear fusion power research, the availability of thermometers for cryogenic temperatures has become more important.[11,12] Recently, several ratiometric thermometers based on lanthanoid metal–organic frameworks (MOFs) have been reported containing a mixture of lanthanide ions, mainly Eu^{III} and Tb^{III}.[8,9,13−24] However, the lack of sensitivity at cryogenic temperatures limits their application. Extending the sensing temperature range to below 50 K is of great value for both cryogenic research and industrial applications, e.g., energy and space exploration. The electronic probes currently used have well-known drawbacks due to contact measurements.[25]

Herein, we report a new metal–organic framework LnHL (H_4L = 5-hydroxy-1,2,4-benzenetricarboxylic acid) containing high concentrations of Ln^{III} ions within 1-D zigzag chains. Notably, on the basis of a mechanism combining both phonon-assisted energy migration and phonon-assisted energy transfer, $Tb_{0.95}Eu_{0.05}HL$ can be used as a ratiometric thermometer even down to 4 K and has remarkable temperature sensitivity up to 31% K^{-1} at 4 K. It is the first time that phonon-assisted energy migration between Ln ions forms the basis of the mechanism of a cryogenic MOF thermometer.

Received: August 20, 2015
Published: November 24, 2015

DOI: 10.1021/acs.inorgchem.5b01924
Inorg. Chem. 2015, 54, 11323−11329

EXPERIMENTAL SECTION

Materials and Methods. Solvent and reagents were commercially available and used without further purification. NMR spectra were recorded on a Bruker DPX-300 spectrometer. Elemental analysis for C and H was performed on a Perkin-Elmer 2400 series II analyzer. Mass spectra were recorded using a Finnigan Aqua mass spectrometer (MS) with electrospray ionization (ESI). IR spectra were recorded with a Perkin-Elmer Paragon 1000 FTIR spectrophotometer equipped with a Golden Gate ATR device. The excitation and emission spectra were measured on a Shimadzu RF-5301PC spectrofluoriphotometer. X-ray powder diffraction patterns were obtained on a Philips PW 1050 diffractometer using Cu Kα radiation (λ = 1.542 Å). Inductively coupled plasma (ICP) emission spectroscopy was performed on a VISTA-MPX Simultaneous TCP-OES with Varian SPS 3 sample preparation system. Thermogravimetric analyses (TGA) spectra were recorded on a NETZSCH STA 499 instrument under argon atmosphere with heating rate of 3 K per minute. Luminescence lifetime was determined using an Edinburg Instruments FLS920 spectrophotometer, with an OPOTEK Opolette 355 HR pulsed laser as the excitation source. Temperature-dependent emission spectra were recorded using an Oxford Instruments liquid helium flow cryostat for the temperature range from 4.2 to 290 K; Hamamatsu R928 PMT is used as a detector. Photoluminescence quantum yields at room temperature were determined using the absolute method.[26] An integrating sphere (Avantes AvaSphere 30REFL) was connected to an irradiance-calibrated CCD spectrometer (Avantes AvaSpec-2048UA). A 1000 W xenon lamp (LOT) and a Spex monochromator were used as the excitation source.

Synthesis of 5-Hydroxy-1,2,4-benzenetricarboxylic Acid (H_4L). The ligand was synthesized using a procedure that was slightly modified from that of the literature.[27,28] Details for 2,4,5-trimethylbenzenesulfonic acid (**1**) follow. With stirring, concentrated sulfuric acid (40 mL, 736 mmol) was added to 1,2,4-trimethylbenzene (20 mL, 146 mmol). After stirring for 30 min, 60 g of ice was added, resulting in the immediate formation of white solid. The product was collected by filtration, and recrystallized from 200 mL of 20% hydrochloric acid to give a light blue crystalline solid. Yield: 21.5 g (74%). ^{1}H NMR (300 MHz, D_2O): δ = 7.58 (s, 1H), 7.11 (s, 1H), 2.47 (s, 1H), 2.21 ppm (s, 2H). ^{13}C NMR (300 MHz, D_2O): δ = 140.2, 137.6, 133.9, 133.2, 132.8, 132.7, 127.3, 18.7, 18.2, 18.0 ppm. IR (ν): 2976 (br), 1691 (br), 1148 (s), 1048 (s), 973 (s), 655(m), 559 (m), 491 (m) cm^{-1}. Mp: 109 °C. ESI-MS found (calcd): 199.1 (199.1) $[M - H]^-$.

Details for 5-sulfo-benzene-1,2,4-tricarboxylic acid (**2**) follow. Solid potassium permanganate (47 g, 159 mmol) was added slowly to a stirred solution of **1** (10 g, 50 mmol) and NaOH (4 g, 100 mmol) in 250 mL of H_2O at 90 °C. The solution was refluxed for 1 day. Then, ethanol (10 mL) was added carefully to discolour the reaction solution. Solid MnO_2 was removed by filtration and was washed with hot water (2 × 100 mL). The filtrate was evaporated in vacuo. The residue was taken up in 40 mL of H_2O, and concentrated hydrochloric acid was added to pH = 1, resulting in the formation of white solid. After stirring for an additional 20 min, the white solid was collected by filtration and dried in vacuo. Yield: 11.9 g (82%). ^{1}H NMR (300 MHz, D_2O): δ = 8.14 (s, 1H), 7.73 ppm (s, 1H). ^{13}C NMR (300 MHz, D_2O): δ = 172.2, 171.9, 171.1, 141.0, 136.5, 135.7, 133.8, 127.9, 127.7 ppm. IR (ν): 3473 (br), 1710 (w), 1450 (m), 1383 (m), 1277 (m), 1241 (m), 1204 (vs), 1039 (vs), 767 (s), 634 (s), 589 (s) cm^{-1}. ESI-MS found (calcd): 289.0 (289.0) $[M - H]^-$, 144.1 (144.0) $[1/2(M - 2H)]^-$.

Details for 5-hydroxy-1,2,4-benzenetricarboxylic acid (H_4L) follow. Compound **2** (11 g, 38 mmol) and KOH (39 g, 695 mmol) were mixed together with 7 mL of water in a 50 mL Teflon vessel. The vessel without cap was put in an oven set at 200 °C for 7 h. Then, the mixture was added to 200 mL of water, and concentrated hydrochloric acid was added to pH = 1. The reaction mixture was heated to boiling for 30 min, and then put in the refrigerator. The white solid formed was collected by filtration and dried in vacuo. Yield: 6.7 g (78%). ^{1}H NMR (300 MHz, D_2O): δ = 8.43 (s, 1H), 7.05 ppm (s, 1H). ^{13}C NMR (300 MHz, CD_3OD): δ = 171.0, 170.3, 167.2, 164.4, 142.1, 133.0, 120.2, 116.5, 113.4 ppm. IR (ν): 3384 (br), 1694 (s), 1579 (m), 1327 (m), 1220 (s), 1137 (m), 859 (m), 757 (s), 635 (s) cm^{-1}. Mp: 237 °C. ESI-MS found (calcd): 225.0 (225.0) $[M - H]^-$, 451.0 (451.0) $[2M - H]^-$.

Hydrothermal Synthesis of the Lanthanoid Compounds. A mixture of H_4L (67.84 mg, 0.3 mmol), $LnCl_3{\cdot}6H_2O$ (0.1 mmol, *Ln* = Tb, Eu), 5 mL of water, and 5 mL of ethanol was brought into a 25 mL Teflon lined stainless steel vessel; the vessel was closed, and a number of reaction vessels together were placed in a big pan containing 15 kg of sand. The reaction vessels were heated for 1 day in an oven set at 120 °C. The oven was slowly cooled down to room temperature at a rate of 2.5 °C/h. Colorless crystals were collected on a glass frit and washed with water and ethanol. Yield: 12 mg (23%) for TbHL and 13 mg (25%) for EuHL based on $LnCl_3{\cdot}6H_2O$.

TbHL analyzed as $\{[Tb_2(HL)_2(H_2O)_3]{\cdot}5.5H_2O\}_n$. Anal. Found (Calcd) for $C_{18}H_{23}O_{22.5}Tb_2$: C, 23.54 (23.57); H, 2.61 (2.53). Selected IR data (ν): 3175 (br), 1546 (s), 1387 (vs), 1264 (s), 884 (m), 805 (m), 656 (s), 566 (s), 475 (m) cm^{-1}.

EuHL analyzed as $\{[Eu_2(HL)_2(H_2O)_3]{\cdot}5.5H_2O\}_n$. Anal. Found (Calcd) for $C_{18}H_{23}Eu_2O_{22.5}$: C, 23.73 (23.93); H, 2.45 (2.57). Selected IR data (ν): 3180 (br), 1544 (s), 1387 (vs), 1263 (s), 881 (m), 803 (m), 656 (s), 564 (s), 471 (m) cm^{-1}.

The synthesis of mixed-lanthanoid compounds was carried out following the procedure described above, but mixtures of $TbCl_3{\cdot}6H_2O$, $EuCl_3{\cdot}6H_2O$, and $GdCl_3{\cdot}6H_2O$ were used instead of pure *Ln* salts. Yields: 13 mg (28%) for $Gd_{0.95}Tb_{0.05}$HL; 12 mg (26%) for $Gd_{0.95}Eu_{0.05}$HL; 12 mg (26%) for $Tb_{0.95}Eu_{0.05}$HL; 12 mg (26%) for $Tb_{0.8}Eu_{0.2}$HL; 10 mg (22%) for $Tb_{0.6}Eu_{0.4}$HL; 11 mg (24%) for $Tb_{0.4}Eu_{0.6}$HL; 12 mg (27%) for $Tb_{0.2}Eu_{0.8}$HL based on Ln salts. Inductively coupled plasma atomic emission spectroscopy (ICP-AES) analysis for Tb, Eu, and Gd (Table S3), and elemental analyses for C and H were used to determine the chemical composition of the compounds.

$Gd_{0.95}Tb_{0.05}$HL analyzed as $\{[Gd_{1.88}Tb_{0.12}(HL)_2(H_2O)_3]{\cdot}5H_2O\}_n$. Anal. Found (Calcd) for $C_{18}H_{22}Gd_{1.88}O_{22}Tb_{0.11}$: C, 23.85 (23.93); H, 2.18 (2.45). Selected IR data (ν, cm^{-1}): 3185 (br), 1547 (s), 1390 (vs), 1265 (s), 883 (m), 805 (m), 656 (s), 566 (s), 475 (m).

$Gd_{0.9}Eu_{0.05}Tb_{0.05}$HL analyzed as $\{[Gd_{1.8}Eu_{0.08}Tb_{0.12}(HL)_2(H_2O)_3]{\cdot}5H_2O\}_n$. Anal. Found (Calcd) for $C_{18}H_{22}Eu_{0.08}Gd_{1.8}O_{22}Tb_{0.12}$: C, 23.96 (23.88); H, 2.18 (2.45). Selected IR data (ν): 3185 (br), 1548 (s), 1391 (vs), 1265 (s), 884 (m), 803 (m), 657 (s), 566 (s), 475 (m) cm^{-1}.

$Gd_{0.95}Eu_{0.05}$HL analyzed as $\{[Gd_{1.82}Eu_{0.18}(HL)_2(H_2O)_3]{\cdot}5H_2O\}_n$. Anal. Found (Calcd) for $C_{18}H_{22}Eu_{0.18}Gd_{1.82}O_{22}$: C, 23.73 (23.92); H, 2.27 (2.45). Selected IR data (ν, cm^{-1}): 3185 (br), 1547 (s), 1390 (vs), 1263 (s), 883 (m), 803 (m), 657 (s), 566 (s), 478 (m).

$Tb_{0.95}Eu_{0.05}$HL analyzed as $\{[Tb_{1.87}Eu_{0.13}(HL)_2(H_2O)_3]{\cdot}5.5H_2O\}_n$. Anal. Found (Calcd) for $C_{18}H_{23}Eu_{0.13}O_{22.5}Tb_{1.87}$: C, 23.58 (23.59); H, 2.34 (2.53). Selected IR data (ν, cm^{-1}): 3187 (br), 1548 (s), 1391 (vs), 1262 (s), 885 (m), 805 (m), 657 (s), 567 (s), 475 (m).

$Tb_{0.8}Eu_{0.2}$HL analyzed as $\{[Tb_{1.55}Eu_{0.45}(HL)_2(H_2O)_3]{\cdot}5H_2O\}_n$. Anal. Found (Calcd) for $C_{18}H_{22}Eu_{0.45}O_{22}Tb_{1.55}$: C, 23.83 (23.89); H, 2.25 (2.45). Selected IR data (ν, cm^{-1}): 3183 (br), 1546 (s), 1388 (vs), 1264 (s), 884 (m), 804 (m), 657 (s), 565 (s), 479 (m).

$Tb_{0.6}Eu_{0.4}$HL analyzed as $\{[Tb_{1.09}Eu_{0.91}(HL)_2(H_2O)_3]{\cdot}5.5H_2O\}_n$. Anal. Found (Calcd) for $C_{18}H_{23}Eu_{0.91}O_{22.5}Tb_{1.09}$: C, 23.93 (23.73); H, 2.36 (2.55). Selected IR data (ν, cm^{-1}): 3173 (br), 1545 (s), 1388 (vs), 1264 (s), 883 (m), 804 (m), 656 (s), 565 (s), 474 (m).

$Tb_{0.4}Eu_{0.6}$HL analyzed as $\{[Tb_{0.72}Eu_{1.28}(HL)_2(H_2O)_3]{\cdot}5.5H_2O\}_n$. Anal. Found (Calcd) for $C_{18}H_{23}Eu_{1.28}O_{22.5}Tb_{0.72}$: C, 23.96 (23.80); H, 2.39 (2.55). Selected IR data (ν, cm^{-1}): 3167 (br), 1545 (s), 1388 (vs), 1264 (s), 882 (m), 804 (m), 656 (s), 564 (s), 474 (m).

$Tb_{0.2}Eu_{0.8}$HL analyzed as $\{[Tb_{0.35}Eu_{1.65}(HL)_2(H_2O)_3]{\cdot}5.5H_2O\}_n$. Anal. Found (Calcd) for $C_{18}H_{22}Eu_{1.65}O_{22}Tb_{0.35}$: C, 24.14 (24.11); H, 2.42 (2.47). Selected IR data (ν, cm^{-1}): 3183 (br), 1545 (s), 1387 (vs), 1264 (s), 882 (m), 804 (m), 656 (s), 564 (s), 474 (m).

Single Crystal Structure Determination. X-ray quality single crystals of TbHL and EuHL were isolated from the procedure described above. The crystals were mounted to a glass fiber using the

DOI: 10.1021/acs.inorgchem.5b01924
Inorg. Chem. 2015, 54, 11323−11329

oil-drop method.[29] The data were collected at 173 K on a Nonius Kappa CCD diffractometer (Mo Kα radiation, λ = 0.710 73 Å). The intensity data were corrected for Lorentz and polarization effects, and for absorption. The programs COLLECT,[30] SHELXS-97,[31] SHELXL-97[32] were used for data reduction, structure solution, and structure refinement, respectively. The non-hydrogen atoms were refined anisotropically. The H atoms were determined at the difference map and refined isotropically riding with the heavy atom connected except water hydrogens where also the coordinates were refined. The unit cell contains 18 water molecules which have been treated as a diffuse contribution to the overall scattering without specific atom positions by SQUEEZE/PLATON.[33]

As a result, there is no electron density of the disordered water molecules in the voids.

RESULTS AND DISCUSSION

Colorless single crystals of TbH**L** and EuH**L** were obtained by reacting $LnCl_3 \cdot 6H_2O$ (Ln^{III} = Eu, Tb) and H_4**L** under hydrothermal conditions.[34] In addition, mixed-lanthanoid samples were synthesized through the same procedure by varying the ratio of *Ln* salts. Powder XRD (Figures S1 and S2) and IR spectra (Figures S3 and S4) show that these compounds all are isostructural. The compounds TbH**L** and EuH**L** crystallize in the monoclinic space group *C*2/*c*; only the structure of TbH**L** is discussed below (Figure 1 and Figures S5 and S6; crystallographic data are provided in Table S1, and selected bond distances and angles are collected in Table S2). The asymmetric unit of TbH**L** comprises one Tb^{III} ion, one triply deprotonated ligand HL^{3-}, and one and a half molecules of water. The nine-coordinated Tb^{III} ion is in a geometry that is best described as a distorted triaugmented triangular prism by the coordination of seven O donors from five carboxylate groups and two O donors from water molecules. The Tb−O distances are in the range 2.26−2.64 Å. Adjacent Tb^{III} ions are connected by two bridging O atoms from carboxyl groups, forming the repeating unit $[Tb_2(COO)_6(H_2O)_3]$. These repeating units are bridged by a water molecule, creating the infinite 1-D zigzag chain $[Tb_2(COO)_6(H_2O)_3]_n$ as the secondary building unit (SBU) along the *c* axis. The adjacent Tb^{III} to Tb^{III} distances are 4.212 and 4.532 Å. The SBUs are connected to four adjacent SBUs via the ligand HL^{3-}, thus generating the 3D framework. A topological analysis of the framework was performed with the program TOPOS.[35,36] Each binuclear SBU unit is considered as a 10-fold connected node. The ligand HL^{3-} serves as a four-connected node, and water acts as bridge (Figure 2). The structure can then be described as a 4,10-connected net, named sqc246. The point symbol for this topology is $\{3^2.4^2.5^2\}_2\{3^8.4^{16}.5^8.6^{13}\}$.

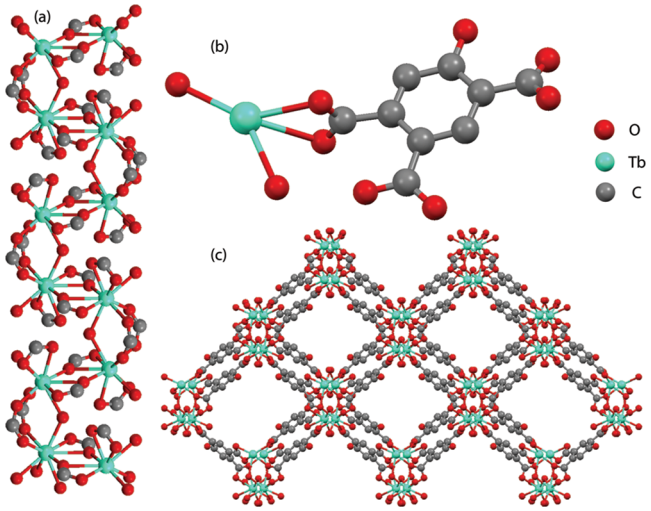

Figure 1. Crystal structure of (a) 1-D Tb chain bridged by carboxylate groups and water and (b) asymmetric unit. (c) Projection of the structure of TbH**L** down the channels along the *c* axis. All hydrogen atoms and disordered water molecules in the channels are not shown. Green = terbium, red = oxygen, gray = carbon.

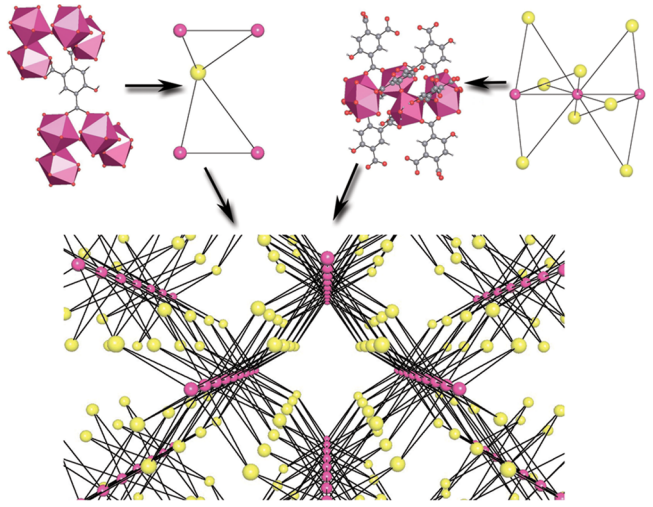

Figure 2. Topological structure of TbH**L**: (pink) repeating units of SBU; (yellow) ligand H**L**.

The framework of TbH**L** contains one-dimensional channels along the [001] direction. The void volume of these channels as calculated by PLATON[33] is 830.4 Å^3 corresponding to 30.3% of the unit cell volume. The channels are filled with approximately 18 disordered water molecules per unit cell. Thermogravimetric analyses (TGA) of TbH**L** and EuH**L** confirm the presence of the water molecules within the 1-D channels (Figure S7). The guest water molecules in the channels are removed at 390 K. About $^2/_3$ of the coordinated water molecules, corresponding to the terminal water molecules, are lost at ca. 430 K. The remaining $^1/_3$ of the coordinated water molecules (the bridging water molecule) are lost at ca. 500 K. The framework starts to decompose at about 635 K. The total weight loss ascribed to water is 16.6%, in agreement with the 16.7% water content calculated from elemental analysis. EuH**L** shows similar thermal behavior; the weight loss of 16.4% is in agreement with the 16.9% water content calculated from elemental analysis.

Upon excitation at 325 nm TbH**L** displays the characteristic emission peaks of the Tb^{III} ion (Figure S8) whereas EuH**L** only shows very weak red emission (Figure S9). The doped compound $Gd_{0.95}Eu_{0.05}$H**L** (containing only 5% europium) exhibits the characteristic emission of the Eu^{III} ion when excited at 325 nm (Figure S10). The excitation spectrum shows a broad-band peak belonging to ligand-centered excitation. This result indicates that the significantly lower emission intensity of pure EuH**L** is due to concentration quenching.[37,38] The triplet energy level of the ligand is estimated to be 26.6 × 10^3 cm^{-1} from the shortest-wavelength phosphorescence band in the phosphorescence spectrum of GdH**L** recorded at 77 K (Figure S11).[39−42] The energy difference between the triplet state of the ligand and the Tb^{III} emitting level ($^5D_4$, 20.5 × 10^3 cm^{-1}) is

DOI: 10.1021/acs.inorgchem.5b01924
Inorg. Chem. 2015, 54, 11323−11329

approximately 6100 cm^{-1}. According to Latva's rules, the energy of the triplet level of the ligand can thus be transferred to Tb^{III} without significant energy back transfer.[39] The mixed-lanthanoid compounds $Tb_xEu_{1-x}HL$ (x = 0.95, 0.8, 0.6, 0.4, 0.2) exhibit the peaks of both Eu^{III} and Tb^{III} ions when excited at 325 nm (Figures S12−14), but the emission intensity is quite low for the compounds with a europium content higher than 40%.

Emission lifetimes were determined for TbHL, $Gd_{0.95}Tb_{0.05}HL$, $Gd_{0.95}Eu_{0.05}HL$, and $Tb_xEu_{1-x}HL$ (x = 0.95, 0.8, 0.6) (Figures S15 and S16); the emissions of EuHL, $Tb_{0.4}Eu_{0.6}HL$, $Tb_{0.2}Eu_{0.8}HL$ are too weak for lifetime measurements. Monoexponential behavior was observed for the $^5D_4$ decay curve monitored at 540 nm for Tb^{III} in TbHL and $Gd_{0.95}Tb_{0.05}HL$. Similar behavior was observed for the $^5D_0$ decay monitored at 615 nm for Eu^{III} in $Gd_{0.95}Eu_{0.05}HL$ and $Tb_xEu_{1-x}HL$ (x = 0.95, 0.8, 0.6). The $^5D_4$ decay curves monitored at 544 nm for Tb^{III} in $Tb_xEu_{1-x}HL$ (x = 0.95, 0.8, 0.6) display nonexponential behavior. These are characterized by average lifetimes as given in eq 1 (Table S4).[43]

$$\tau = \frac{\int_0^\infty I(t)t\,dt}{\int_0^\infty I(t)\,dt} \quad (1)$$

The decay curves of Eu^{III} in $Tb_xEu_{1-x}HL$ (x = 0.95, 0.8, 0.6) exhibit a build-up before decay, indicating the occurrence of Tb^{III} to Eu^{III} energy transfer (Figure S15). It is clear that the rise time decreases with increasing fraction of Eu^{III}. The lifetime of Eu^{III} emission decreases slightly with increasing the Eu^{III} concentrations (Table S4). The energy-transfer probability P from Tb^{III} to Eu^{III} can be calculated by $P = 1/\tau - 1/\tau_0$, and the energy-transfer efficiency can be calculated with $\eta = 1 - \tau/\tau_0$, where τ_0 and τ are the lifetimes of terbium emissions in TbHL and the Eu-doped compounds, respectively.[15,44] As shown in Table S4, the energy-transfer efficiency increases with increasing concentrations of Eu^{III} for $Tb_xEu_{1-x}HL$ (x = 0.95, 0.8, 0.6).

In order to gain better understanding of the mechanisms governing the energy transfer, the temperature dependence of luminescence emission of $Tb_{0.95}Eu_{0.05}HL$ was also studied (Figure 3). With an increase in the temperature from 4 to 290 K, the emission intensity of Tb^{III} decreases while Eu^{III} intensity increases. A plot of the emission intensity ratio of the $^5D_0 \rightarrow {}^7F_2$ (Eu^{III}, 615 nm) and $^5D_4 \rightarrow {}^7F_5$ (Tb^{III}, 540 nm) transitions as a function of temperature is shown in Figure 4 (■). Interestingly, especially in the low temperature range from 4 to 50 K, an increase of the temperature leads to rapid decrease of the Tb^{III} emission intensity accompanied by a fast increase of Eu^{III} emission intensity. These dramatic intensity changes allow the use of our compound as a potential thermometer at cryogenic temperatures.

The ratiometric thermometric parameter y is defined as the ratio of the emission intensity of the $^5D_0 \rightarrow {}^7F_2$ (Eu^{III}) and $^5D_4 \rightarrow {}^7F_5$ (Tb^{III}) transitions. The relationship between y and temperature T was fitted with eq 2 in the temperature range 4−290 K. The correlation coefficient is R^2 = 0.996.

$$y = -1.966 + 0.895\ln(T + 6.965) \quad (4 < T < 290) \quad (2)$$

The relative sensitivity and temperature uncertainty are often used to characterize the thermometer performance.[20,23] The relative sensitivity (S_r) is defined as dy/ydT (see Figure 4 for details). The results show that this novel ratiometric thermometer can be used in a wide temperature range, and it is especially sensitive in the range 4−50 K, having a high relative sensitivity up to 31% K^{-1} at 4 K. A comprehensive comparison of this work and other reported ratiometric thermometers is provided in Table S5 and Figure S17. The accuracy of our compound is excellent, as judged from the correlation coefficient R^2 of the fitting curve.[20,45] The temperature uncertainty is estimated by the equation $\delta T = (1/S_r)(\delta y/y)$, in which $\delta y/y$ is the relative uncertainty of thermometer parameter determination and S_r is the relative sensitivity. In our case $\delta y/y$ is about 0.5%, a typical value for portable detectors.[23,46,47] The temperature uncertainty is shown in Figure S18, and it is 0.02 at 4 K, and 1.31 at 100 K, respectively.

The stability of $Tb_{0.95}Eu_{0.05}HL$ as a thermometer was tested by exposing the compound to repeated heating and cooling cycles first from 110 to 4 K four times and then from 290 to

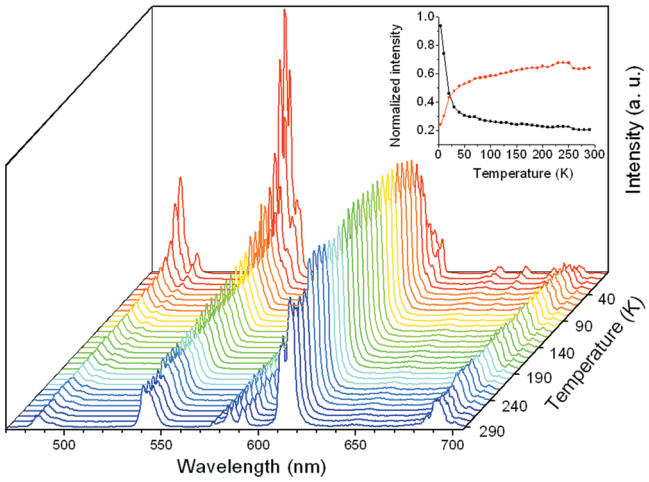

Figure 3. Emission spectra of $Tb_{0.95}Eu_{0.05}HL$ in the solid state in the temperature range 4−290 K (λ_{ex} = 325 nm). Inset: temperature-dependent luminescence intensity of $^5D_0 \rightarrow {}^7F_2$ (red, Eu^{III} at 615 nm) and $^5D_4 \rightarrow {}^7F_5$ (black, Tb^{III} at 540 nm) transition in $Tb_{0.95}Eu_{0.05}HL$ (λ_{ex} = 325 nm).

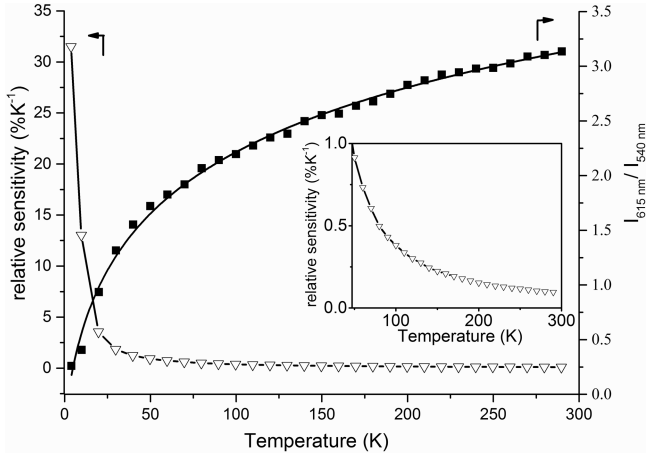

Figure 4. Emission intensity ratio of the $^5D_0 \rightarrow {}^7F_2$ (Eu^{III}, 615 nm) and $^5D_4 \rightarrow {}^7F_5$ (Tb^{III}, 540 nm) transitions for $Tb_{0.95}Eu_{0.05}HL$ as a function of temperature (■, right axis) with the fitting curve (black line; R^2 = 0.996) and the relative sensitivity curve (▽, left axis). Inset: Enlarged relative sensitivity curve from 50 to 300 K.

DOI: 10.1021/acs.inorgchem.5b01924
Inorg. Chem. 2015, 54, 11323−11329

110 K four times (Figure S19). The response of the emission spectrum to changes in temperature appeared to be fully reversible. Furthermore, the powder XRD pattern of $Tb_{0.95}Eu_{0.05}$HL after low temperature emission measurement is similar to the one taken before low temperature measurement (Figure S2). The IR spectra of $Tb_{0.95}Eu_{0.05}$HL before and after the low temperature measurements are also highly similar (Figure S4).

The dramatic luminescence color change of $Tb_{0.95}Eu_{0.05}$HL in the temperature range 4−50 K thus makes it a promising colorimetric thermometer for in situ temperature measurements. The CIE (Commission International d'Elairage) chromaticity diagram coordinates have been calculated on the basis of the corresponding emission spectra from 4 to 50 K. The luminescence color of $Tb_{0.95}Eu_{0.05}$HL changes from green (X = 0.347, Y = 0.570) at 4 K to yellow/red (X = 0.507, Y = 0.453) at 50 K (Figure S20). This color change can be clearly observed by the eyes.

The emission intensities of the Eu^{III} and Tb^{III} centers in the doped compound $Gd_{0.90}Eu_{0.05}Tb_{0.05}$HL containing 5% Tb and 5% Eu change only slightly in the whole temperature range; at lower temperatures the phosphorescence band of the ligand becomes more prominent. This indicates that the temperature-dependent emission of $Tb_{0.95}Eu_{0.05}$HL is related to the absolute Eu^{III} and Tb^{III} concentrations and their mutual interactions (Figure 5). The excitation spectra of $Tb_{0.95}Eu_{0.05}$HL (monitored at the emission of Eu^{III} at 615 nm) in the temperature range 4−290 K apart from a broad band for ligand-centered excitation all show the direct excitation of Tb^{III} (Figure S21). The initial rise in all the decay curves of the $^5D_0 \rightarrow {}^7F_2$ transition (Eu^{III} at 615 nm) in $Tb_{0.95}Eu_{0.05}$HL (Figure 6a) indicates that energy transfer of Tb^{III} to Eu^{III} occurs in the whole temperature range. The lifetime of the Tb^{III} emission in $Tb_{0.95}Eu_{0.05}$HL decreases dramatically from 4 to 50 K, and the decay curve changes from monoexponential to nonexponential (Figure 6b and Figure S22). The lifetime of the Eu^{III} emission in $Tb_{0.95}Eu_{0.05}$HL decreases only slightly (Figure 6a and Figure S22). These results indicate that the probability of energy transfer from Tb^{III} to Eu^{III} centers changes dramatically as the temperature increases. At room temperature, the lifetime of Tb emission in $Gd_{0.95}Tb_{0.05}$HL is 0.824 ms. This value is very close to the Tb lifetime in TbHL at 4 K (0.865 ms; Tables S4 and S6). At temperatures higher than 30 K, the Tb lifetimes in TbHL are below 0.754 ms. These observations indicate that the energy migration between Tb centers in TbHL occurs more efficiently when the temperature is higher than 4 K. At 4 K, the lifetime of Tb emission in $Tb_{0.95}Eu_{0.05}$HL (0.858 ms) is very close to that in pure TbHL (0.865 ms). However, at 30 K the lifetime of Tb emission in $Tb_{0.95}Eu_{0.05}$HL becomes 0.383 ms, about half that found for the pure TbHL at 30 K (0.754 ms). Due to the larger energy gap between Tb^{III} and Eu^{III}, the phonon-assisted energy transfer from Tb to Eu needs larger phonon energy than the phonon-assisted energy migration between Tb centers. The abrupt change in the lifetime of Tb emission in $Tb_{0.95}Eu_{0.05}$HL indicates the occurrence of phonon-assisted energy migration between Tb ions, ultimately resulting in Tb to Eu energy transfer.

On the basis of the results and the similar performance reported for inorganic lanthanide materials,[48−53] we propose that the dramatic changes in the emission intensities of Eu^{III} and Tb^{III} in $Tb_{0.95}Eu_{0.05}$HL in the temperature range 4−50 K are due to changes in the energy-migration efficiency between Tb^{III} ions. Due to small variations in the energy levels of the Tb^{III} center caused by subtle differences in the local surroundings, energy migration between neighboring Tb^{III} ions is hampered at cryogenic temperatures. Low energy phonons are needed to make up the small energy mismatch between neighboring Tb^{III} ions. When the temperature increases from 4 to 50 K, the energy in the excited state of Tb^{III} has more opportunity to migrate to a Tb^{III} ion neighboring a Eu^{III} center, which is followed by subsequent

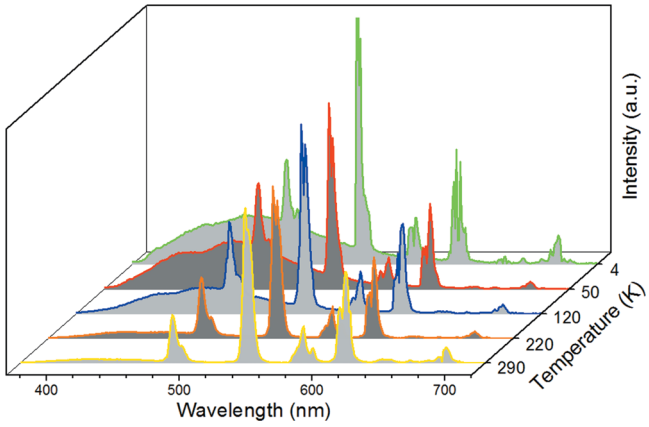

Figure 5. Emission spectra of $Gd_{0.9}Eu_{0.05}Tb_{0.05}$HL in the solid state in the temperature range 4−290 K (λ_{ex} = 325 nm).

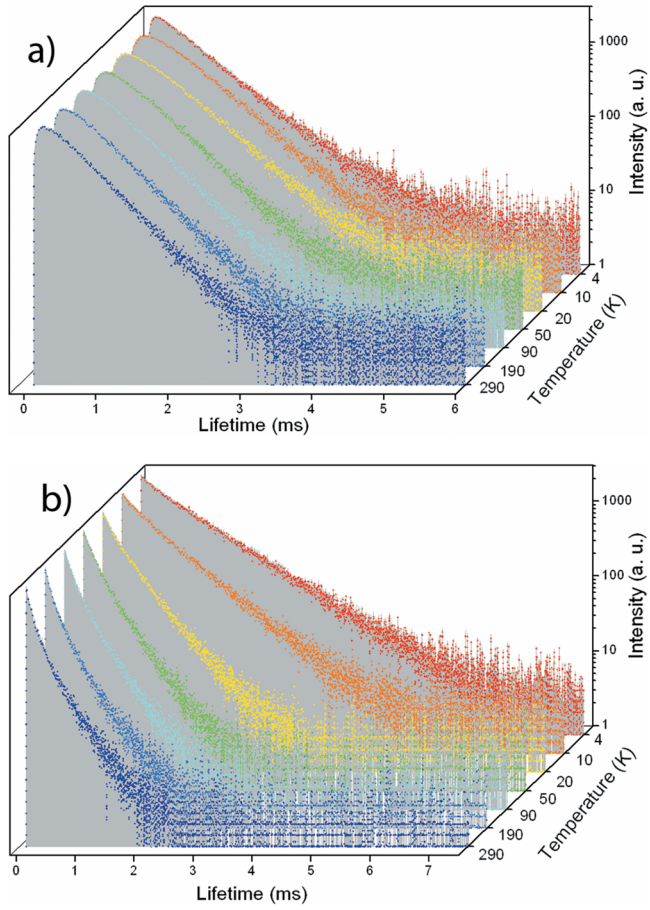

Figure 6. Luminescence decay curves of (a) the $^5D_0 \rightarrow {}^7F_2$ (Eu^{III} at 615 nm) transition and (b) the $^5D_4 \rightarrow {}^7F_5$ (Tb^{III} at 540 nm) transition in $Tb_{0.95}Eu_{0.05}$HL recorded at different temperatures (λ_{ex} = 355 nm).

DOI: 10.1021/acs.inorgchem.5b01924
Inorg. Chem. 2015, 54, 11323−11329

energy transfer to Eu^{III}. This proposed mechanism indicates that the presence of Ln chains and the short *Ln*−*Ln* distances in the structure play an important role in the sensing process at cryogenic temperatures. The slow increase of the Eu^{III} emission intensity and the further decrease of the Tb^{III} emission intensity in the range 50−290 K can be explained by phonon-assisted energy transfer from Tb^{III} to Eu^{III} ions, which is temperature sensitive.[54]

The energy-transfer probability *P* and the energy-transfer efficiency from Tb^{III} to Eu^{III} in $Tb_{0.95}Eu_{0.05}$**HL** were calculated (Table S6): both increase dramatically on going from 4 to 50 K, and then change slightly in the range 50−290 K.

CONCLUSIONS

In summary, we have synthesized a metal−organic framework that can be used as a thermometer in cryogenic temperatures: the working mechanism relies on both phonon-assisted energy migration and phonon-assisted energy-transfer mechanisms. The compound $Tb_{0.95}Eu_{0.05}$**HL** shows a quantum yield of 22% (excited at 325 nm) at room temperature and can be used as an excellent temperature sensor in the wide temperature range 4−290 K, with especially good sensitivity in the range 4−50 K, and with a relative sensitivity up to 31% K^{-1} at 4 K.

ASSOCIATED CONTENT

Supporting Information

The Supporting Information is available free of charge on the ACS Publications website at DOI: 10.1021/acs.inorgchem.5b01924.

Tables of crystal data, bond distances and angles, tables of lifetime data, ICP, PXRD, IR, TGA, excitation and emission spectra, phosphorescence spectrum, and CIE chromaticity diagram (PDF)

AUTHOR INFORMATION

Corresponding Author

*E-mail: bouwman@chem.leidenuniv.nl.

Notes

The authors declare no competing financial interest.

ACKNOWLEDGMENTS

X.L. gratefully acknowledges a grant from the Chinese Scholarship Council (no. 201206250014). We are grateful to Mr. John van Dijk for mass spectrometry and Mr. Jos van Brussel for ICP and elemental analysis.

REFERENCES

(1) Dou, Z. S.; Yu, J. C.; Cui, Y. J.; Yang, Y.; Wang, Z. Y.; Yang, D.; Qian, G. D. *J. Am. Chem. Soc.* **2014**, *136*, 5527−5530.
(2) Wang, X. D.; Wolfbeis, O. S.; Meier, R. J. *Chem. Soc. Rev.* **2013**, *42*, 7834−7869.
(3) Hu, Z. C.; Deibert, B. J.; Li, J. *Chem. Soc. Rev.* **2014**, *43*, 5815−5840.
(4) Zhu, Y.; Wang, Y. M.; Liu, P.; Xia, C. K.; Wu, Y. L.; Lu, X. Q.; Xie, J. M. *Dalton Trans.* **2015**, *44*, 1955−1961.
(5) Meyer, L. V.; Schonfeld, F.; Muller-Buschbaum, K. *Chem. Commun.* **2014**, *50*, 8093−8108.
(6) Seyed-Yagoobi, J. *Rev. Sci. Instrum.* **1991**, *62*, 249−250.
(7) Carlos, L. D.; Ferreira, R. A. S.; de Zea Bermudez, V.; Julian-Lopez, B.; Escribano, P. *Chem. Soc. Rev.* **2011**, *40*, 536−549.
(8) Rao, X. T.; Song, T.; Gao, J. K.; Cui, Y. J.; Yang, Y. Y.; Wu, C. D.; Chen, B. L.; Qian, G. D. *J. Am. Chem. Soc.* **2013**, *135*, 15559−15564.
(9) Cui, Y. J.; Xu, H.; Yue, Y. F.; Guo, Z. Y.; Yu, J. C.; Chen, Z. X.; Gao, J. K.; Yang, Y.; Qian, G. D.; Chen, B. L. *J. Am. Chem. Soc.* **2012**, *134*, 3979−3982.
(10) Brites, C. D. S.; Lima, P. P.; Silva, N. J. O.; Millan, A.; Amaral, V. S.; Palacio, F.; Carlos, L. D. *New J. Chem.* **2011**, *35*, 1177−1183.
(11) Jiang, S. D.; Liu, J. Q.; Yang, B.; Zhu, H. Y.; Yang, C. S. *Microsyst. Technol.* **2014**, *20*, 451−456.
(12) Yamada, H.; Tanaka, Y.; Ogata, M.; Mizuno, K.; Nagashima, K.; Okumura, S.; Terada, Y. *Phys. C* **2011**, *471*, 1570−1575.
(13) Zhao, S. N.; Li, L. J.; Song, X. Z.; Zhu, M.; Hao, Z. M.; Meng, X.; Wu, L. L.; Feng, J.; Song, S. Y.; Wang, C.; Zhang, H. J. *Adv. Funct. Mater.* **2015**, *25*, 1463−1469.
(14) Ramya, A. R.; Sharma, D.; Natarajan, S.; Reddy, M. L. P. *Inorg. Chem.* **2012**, *51*, 8818−8826.
(15) Cadiau, A.; Brites, C. D. S.; Costa, P. M. F. J.; Ferreira, R. A. S.; Rocha, J.; Carlos, L. D. *ACS Nano* **2013**, *7*, 7213−7218.
(16) D'Vries, R. F.; Alvarez-Garcia, S.; Snejko, N.; Bausa, L. E.; Gutierrez-Puebla, E.; de Andres, A.; Monge, M. A. *J. Mater. Chem. C* **2013**, *1*, 6316−6324.
(17) Miyata, K.; Konno, Y.; Nakanishi, T.; Kobayashi, A.; Kato, M.; Fushimi, K.; Hasegawa, Y. *Angew. Chem., Int. Ed.* **2013**, *52*, 6413−6416.
(18) Cui, Y. J.; Zou, W. F.; Song, R. J.; Yu, J. C.; Zhang, W. Q.; Yang, Y.; Qian, G. D. *Chem. Commun.* **2014**, *50*, 719−721.
(19) Han, Y. H.; Tian, C. B.; Li, Q. H.; Du, S. W. *J. Mater. Chem. C* **2014**, *2*, 8065−8070.
(20) Zhou, Y.; Yan, B.; Lei, F. *Chem. Commun.* **2014**, *50*, 15235−15238.
(21) Cui, Y. J.; Song, R. J.; Yu, J. C.; Liu, M.; Wang, Z. Q.; Wu, C. D.; Yang, Y.; Wang, Z. Y.; Chen, B. L.; Qian, G. D. *Adv. Mater.* **2015**, *27*, 1420−1425.
(22) Shen, X.; Lu, Y.; Yan, B. *Eur. J. Inorg. Chem.* **2015**, *2015*, 916−919.
(23) Wang, Z. P.; Ananias, D.; Carné-Sánchez, A.; Brites, C. D. S.; Imaz, I.; Maspoch, D.; Rocha, J.; Carlos, L. D. *Adv. Funct. Mater.* **2015**, *25*, 2824−2830.
(24) Wei, Y. Q.; Sa, R. J.; Li, Q. H.; Wu, K. C. *Dalton Trans.* **2015**, *44*, 3067−3074.
(25) Ylöstalo, J.; Berglund, P.; Niinikoski, O.; Voutilainen, R. *Cryogenics* **1996**, *36*, 1033−1038.
(26) Mello, J. C. d.; Wittmann, H. F.; Friend, R. *Adv. Mater.* **1997**, *9*, 230−232.
(27) Buehler, C. A.; Spees, R. B.; Sanguinetti, P. A. *J. Am. Chem. Soc.* **1949**, *71*, 11−13.
(28) Smith, L. I.; Cass, O. W. *J. Am. Chem. Soc.* **1932**, *54*, 1603−1609.
(29) Kottke, T.; Stalke, D. *J. Appl. Crystallogr.* **1993**, *26*, 615−619.
(30) *COLLECT*; Nonius BV: Delft, The Netherlands, 2002.
(31) Sheldrick, G. M. *SHELXS97*; Bruker AXS Inc.: Madison, WI, 1997.
(32) Sheldrick, G. *Acta Crystallogr., Sect. A: Found. Crystallogr.* **2008**, *64*, 112−122.
(33) Spek, A. *Acta Crystallogr., Sect. D: Biol. Crystallogr.* **2009**, *65*, 148−155.
(34) CCDC 1030166 and CCDC 1030167 contain the supplementary crystallographic data for this Article. These data can be obtained free of charge from The Cambridge Crystallographic Data Centre via www.ccdc.cam.ac.uk/data_request/cif.
(35) Blatov, V. A. *Struct. Chem.* **2012**, *23*, 955−963.
(36) Blatov, V. A.; Shevchenko, A. P.; Proserpio, D. M. *Cryst. Growth Des.* **2014**, *14*, 3576−3586.
(37) Cui, Y. J.; Yue, Y. F.; Qian, G. D.; Chen, B. L. *Chem. Rev.* **2012**, *112*, 1126−62.
(38) Freslon, S.; Luo, Y.; Calvez, G.; Daiguebonne, C.; Guillou, O.; Bernot, K.; Michel, V.; Fan, X. *Inorg. Chem.* **2014**, *53*, 1217−1228.
(39) Latva, M.; Takalo, H.; Mukkala, V. M.; Matachescu, C.; Rodriguez-Ubis, J. C.; Kankare, J. *J. Lumin.* **1997**, *75*, 149−169.
(40) Sager, W. F.; Filipescu, N.; Serafin, F. A. *J. Phys. Chem.* **1965**, *69*, 1092−1100.

DOI: 10.1021/acs.inorgchem.5b01924
Inorg. Chem. 2015, 54, 11323−11329

(41) Dawson, W. R.; Kropp, J. L.; Windsor, M. W. *J. Chem. Phys.* **1966**, *45*, 2410−2418.
(42) Crosby, G. A.; Whan, R. E.; Alire, R. M. *J. Chem. Phys.* **1961**, *34*, 743−748.
(43) van Driel, A. F.; Nikolaev, I. S.; Vergeer, P.; Lodahl, P.; Vanmaekelbergh, D.; Vos, W. L. *Phys. Rev. B: Condens. Matter Mater. Phys.* **2007**, *75*, 035329.
(44) Ananias, D.; Kostova, M.; Almeida Paz, F. A.; Ferreira, A.; Carlos, L. D.; Klinowski, J.; Rocha, J. *J. Am. Chem. Soc.* **2004**, *126*, 10410−10417.
(45) Zhou, Y.; Yan, B. *J. Mater. Chem. C* **2015**, *3*, 9353−9358.
(46) Balabhadra, S.; Debasu, M. L.; Brites, C. D. S.; Nunes, L. A. O.; Malta, O. L.; Rocha, J.; Bettinelli, M.; Carlos, L. D. *Nanoscale* **2015**, *7*, 17261−17267.
(47) Ren, M.; Brites, C. D. S.; Bao, S. S.; Ferreira, R. A. S.; Zheng, L. M.; Carlos, L. D. *J. Mater. Chem. C* **2015**, *3*, 8480−8484.
(48) Buijs, M.; Blasse, G. *J. Lumin.* **1986**, *34*, 263−278.
(49) Buijs, M.; van Vliet, J. P. M.; Blasse, G. *J. Lumin.* **1986**, *35*, 213−222.
(50) Miyakawa, T.; Dexter, D. L. *Phys. Rev. B* **1970**, *1*, 2961−2969.
(51) Yamada, N.; Shionoya, S.; Kushida, T. *J. Phys. Soc. Jpn.* **1972**, *32*, 1577−1586.
(52) dos Santos, P. V.; Gouveia, E. A.; de Araujo, M. T.; Gouveia-Neto, A. S.; Sombra, A. S. B.; Medeiros Neto, J. A. *Appl. Phys. Lett.* **1999**, *74*, 3607−3609.
(53) Macedo, A. G.; Ferreira, R. A. S.; Ananias, D.; Reis, M. S.; Amaral, V. S.; Carlos, L. D.; Rocha, J. *Adv. Funct. Mater.* **2010**, *20*, 624−634.
(54) Auzel, F. *Chem. Rev.* **2004**, *104*, 139−174.

DOI: 10.1021/acs.inorgchem.5b01924
Inorg. Chem. 2015, 54, 11323−11329